8376–8384 *Nucleic Acids Research, 2016, Vol. 44, No. 17* *Published online 28 July 2016*
doi: 10.1093/nar/gkw666

DNA binding proteins explore multiple local configurations during docking via rapid rebinding

Mahipal Ganji[1], Margreet Docter[1], Stuart F.J. Le Grice[2] and Elio A. Abbondanzieri[1,*]

[1]Kavli Institute of Nanoscience, Department of Bionanoscience, TU Delft, 2629HZ, Delft, The Netherlands and [2]Basic Research Laboratory, National Cancer Institute, Frederick, MD 21702, USA

Received March 14, 2016; Revised June 13, 2016; Accepted July 12, 2016

ABSTRACT

Finding the target site and associating in a specific orientation are essential tasks for DNA-binding proteins. In order to make the target search process as efficient as possible, proteins should not only rapidly diffuse to the target site but also dynamically explore multiple local configurations before diffusing away. Protein flipping is an example of this second process that has been observed previously, but the underlying mechanism of flipping remains unclear. Here, we probed the mechanism of protein flipping at the single molecule level, using HIV-1 reverse transcriptase (RT) as a model system. In order to test the effects of long-range attractive forces on flipping efficiency, we varied the salt concentration and macromolecular crowding conditions. As expected, increased salt concentrations weaken the binding of RT to DNA while increased crowding strengthens the binding. Moreover, when we analyzed the flipping kinetics, i.e. the rate and probability of flipping, at each condition we found that flipping was more efficient when RT bound more strongly. Our data are consistent with a view that DNA bound proteins undergo multiple rapid re-binding events, or short hops, that allow the protein to explore other configurations without completely dissociating from the DNA.

INTRODUCTION

Proteins that non-covalently bind and release nucleic acids must undergo a complex three-dimensional search to find specific targets in the crowded environment of the cell. On distance scales of microns to nanometers, this search on long nucleic acid duplexes can be facilitated by a combination of sliding (continuous attachment) and hopping (short three dimensional excursions) (1–3). However, as a protein approaches its target, it must become precisely oriented relative to the target site within the nucleic acid substrate in order to perform enzymatic reactions. These last steps of the target search involve diffusion over nanometer distances, and therefore occur at microsecond to millisecond time scales that are both too fast to observe directly with many experimental techniques and too slow to easily simulate using all-atom molecular dynamics approaches.

Protein flipping has recently emerged as an important component of the last steps of the target search mechanism and in the subsequent exploration of alternate local configurations. It has been proposed that type II restriction enzymes use a flipping mechanism to cleave complementary DNA strands during a single encounter with the target sequence (4–6) and the homeodomain transcription factor HoxD9 was observed to flip to bind on two oppositely oriented binding sites within a single DNA molecule (7). Additionally, flipping was directly observed in single molecule complexes of HIV reverse transcriptase (RT) bound to various nucleic acid substrates (8–10). Furthermore, protein flipping was used as a tool to discriminate between nucleoside and non-nucleoside RT inhibitors (11,12). Flipping requires the enzyme to rotate around a vector perpendicular to the axis of the duplex and is distinct from rotation along the nucleic acid helix (13). Because of this, during a flipping event many specific contacts must be disrupted between the protein and nucleic acid and then immediately reformed with the positions of the two nucleic acid strands in the duplex reversed.

We have chosen RT as a model system to understand the mechanism of flipping using the technique of single-molecule FRET (smFRET). The time resolution of smFRET can be pushed as high as a few milliseconds with high illumination intensities (14) but at a cost of increasing the rate of photo-bleaching (15). Instead of attempting to measure the FRET efficiency during the short-lived flipping intermediates, we chose to measure the rate constant of flipping (k_f), dissociation (k_{off}) and binding (k_{on}) of RT on DNA substrates to decipher the mechanism of the transitions. We therefore selected a frame rate and laser intensity that provides relatively high spatio-temporal resolution (∼1 nm and 100 ms) while allowing us to capture the entire interaction of RT with the DNA with minimal photo-bleaching (∼10%).

*To whom correspondence should be addressed. Tel: +31 152789245; Fax: +31 152781202; Email: e.a.abbondanzieri@tudelft.nl

We have taken advantage of two experimental parameters that modify the affinity of RT for DNA: salt concentration and macromolecular crowding. Low salt concentrations preferentially strengthen the stability of bound states containing strong electrostatic interactions, while crowding agents preferentially strengthen the stability of states that form a compact complex. In other DNA polymerases, the bound states are stabilized by a decrease in the salt concentration of the buffer (16,17) or an increase in macromolecular crowding (18–22). However, the magnitude of this effect on the bound states of RT still remains to be experimentally determined. Typical *in vitro* measurements of RT are frequently performed at low salt concentrations (<50 mM) whereas concentrations of ∼150 mM better mimic the binding interactions observed *in vivo* (23).

Furthermore, using transition state theory we can correlate changes in k_f and k_{off} with changes in the free energy barriers associated with these transitions. Therefore, by measuring how the rate constants and equilibrium constants associated with binding, flipping and dissociation change as a function of salt and macromolecular crowding, we can determine the relative stability of each transition state.

For a given bound state (B) and an associated flipped bound state (F), we consider two possible mechanisms for flipping to occur which we define as 'tumbling' and 'hopping' (Supplementary Figure S1). In the tumbling model (Figure 1A, left), the enzyme maintains some non-covalent contacts with substrate during the flipping transition and the complex becomes slightly less compact (Supplementary Figure S1). The flipping transition by tumbling is therefore distinct from the dissociation transition. Tumbling can be thought of as an analog to the sliding transition that has been shown to mediate one-dimensional diffusion of proteins on DNA (13,24,25). In the hopping model (Figure 1A, right), the enzyme enters a short-lived pseudo-bound intermediate state representing the short diffusive excursions near the DNA that allow flipping or dissociation to occur (Supplementary Figure S1). A pseudo-bound state (or 'effective' state) has been previously introduced to capture the essential kinetic behavior of diffusing macromolecules undergoing competitor-induced dissociation (26). An analogous hopping transition has been shown to allow some proteins to diffuse along DNA (27,28).

If flipping occurs by tumbling, we expect that RT breaks electrostatic contacts and becomes less compact in the tumbling transition state. We therefore would expect that k_f would decrease as salt concentration decreases or macromolecular crowding increases. However, if flipping occurs by hopping, k_f will be affected by both the rate at which RT enters into the less compact pseudo-bound state and the probability that the enzyme rebinds from the pseudo-bound state rather than dissociating. If the long-range (0–2 nm) attractive forces between the enzyme and the DNA increase, the rate of entering the pseudo-bound state will decrease but the likelihood of rebinding will increase, making it possible that the net k_f could increase (Supplementary Material and Supplementary Figure S7). Below we show that changes in k_f and flipping probability (P_{flip}) can be explained by the hopping model but not the tumbling model.

MATERIALS AND METHODS

Labeled RT and nucleic acid substrates preparation

Individual subunits of HIV-1 RT were expressed separately as described earlier (29). An E478Q mutation was introduced in p66 subunit to eliminate RNase H activity (30). To allow for site-specific labeling, native cysteines in the p66 subunit were converted to serine and a unique cysteine was introduced at its C-terminus (31). All purification steps were performed at 4°C. As a first round of purification, p66 was expressed and purified via a self-poured Ni-NTA (GE Healthcare) column. The resultant p66 was applied to a heparin-Sepharose column (GE Healthcare). The enzyme was reduced with DTT on the column and then the column was washed with 50 ml of DTT free sodium phosphate buffer. Reduced p66 was eluted by applying a 75 mM–1M NaCl gradient and purified protein was immediately mixed with Cy3-maleimide dye (GE Healthcare) at a 1:10 protein:dye ratio. The labeling reaction was allowed to continue for ∼2 h at room temperature before quenching with a 10-fold molar excessive of 2-mercaptoethanol. The resultant mixture of p66 and Cy3 was loaded onto the heparin-Sepharose column while tracking Cy3 absorption at 550 nm. The column was washed with sodium phosphate buffer, until free dye was removed. Cy3-labeled p66 was then eluted by applying a salt gradient. Labeled protein was concentrated by mono-S chromatography (GE Healthcare). The reaction resulted in ∼50% labeled p66 with >95% purity as observed from absorption and SDS-PAGE analysis, respectively. Functional RT heterodimers of p66 and p51 were prepared by mixing a 1:10 rati6o of p66-Cy3:p51. The mixture was incubated at 37°C for 2 h and then for 4 h at room temperature. The dissociation rates of p51/p51 or p66/p66 homodimers are fast enough compared to p66/p51 heterodimer to allow most to exchange within 6 h (32). Because the concentration of individual subunits is much higher than the dissociation constant (K_d< 10 nM) of heterodimer, we expect to have a majority of p66 in the form of heterodimer. Aliquots were stored at −80°C until just before the measurements. Since p51 alone has low affinity for DNA, excess of p51 does not interfere with heterodimer RT binding to DNA.

DNA substrates were purchased from IDT technologies(IDT; Coralville, IA, USA). Where applicable, a thymine nucleotide was amino modified with C6 linker, in order to label oligonucleotides with an acceptor fluorophore. Mono-reactive Cy5 (GE healthcare) was attached to an amine group on the nucleic acids as described by the manufacturer. Excess non-reactive dye was removed by ethanol precipitation. Absorption measurements indicate that the labeling efficiency was close to 100%. A 1:10 ratio mixture of the complementary strands with biotin modifications at their 5′-end were annealed to Cy5-labeled strand by heating at 80°C for 5 min and allowed to cool to room temperature. The annealing buffer was 100 mM Tris-HCl (pH 8.0), 1 mM EDTA and 100 mM NaCl. The product was stored at −20°C.

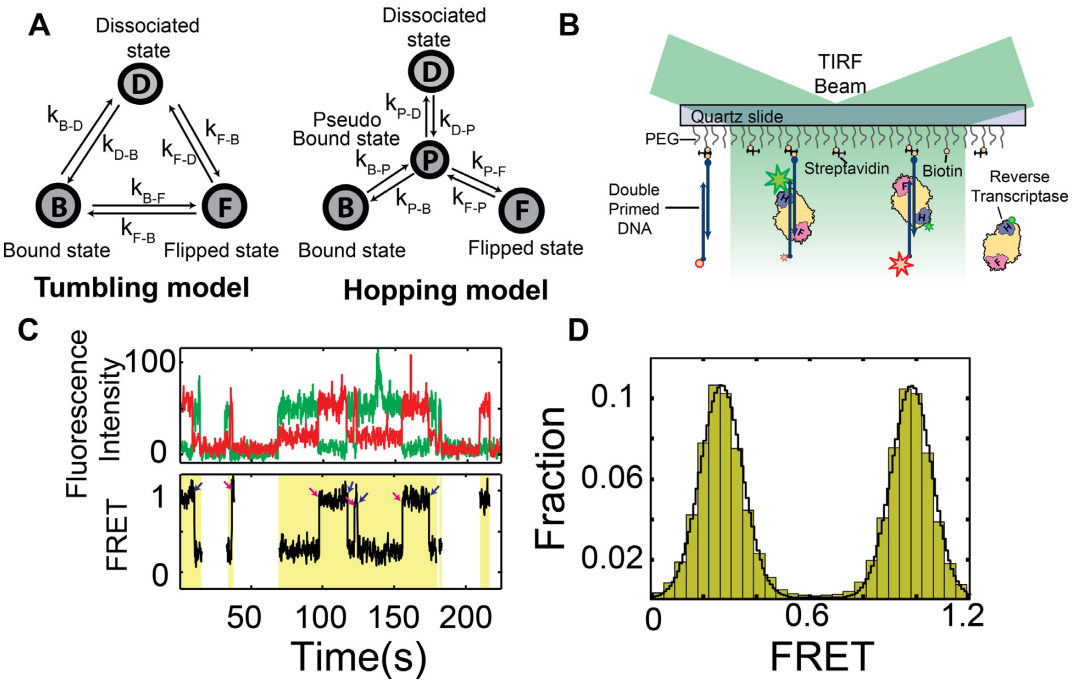

Figure 1. Single-molecule FRET assay for probing RT dynamics. (**A**) Two possible models describing flipping transition ***left***- tumbling model, a basic three state model in which RT can undergo a transition of flipping or dissociation from a bound state and ***right***- hopping model, a model with a pseudo bound state in which RT must undergo to the transition of flipping or dissociation through the pseudo state. (**B**) Schematic diagram of detection of two binding orientations of RT on a double primer DNA substrate. Larger green star and smaller red star represent a low FRET binding mode, larger red star and smaller green star represent a high FRET binding mode of freely diffusing Cy3(green sphere)-labeled RT to surface immobilized Cy5(red sphere)-labelled DNA. (**C**) FRET analysis of RT binding to a double-primer DNA substrate. Top: fluorescence time traces of Cy3 (green) and Cy5 (red) under 532 nm laser excitation. Bottom: FRET value calculated over the duration of the binding events. Arrows represent low-to-high (pink) and high-to-low(blue) FRET flipping events. Yellow shaded region identifies the bound state and (**D**) FRET distribution histogram of RT binding on 19-bp double primer DNA at 50 mM NaCl. The histogram was constructed from 1534 binding events.

Monitoring the flipping of RT by single-molecule FRET assay

Microscope quartz slides (G. Finkenbeiner, Inc.) and cover slips were passivated with PEG as described (33). Surface passivated slides, together with cover slips, were stored under inert conditions at −80°C until used.

Flow cells were assembled by sandwiching double-sided tape between a cover slip and a quartz slide. Typically the volume of the flow cell was ≤10 μl. A total of 100 μl of buffer A (50 mM Tris-HCl, pH 8.0, 50 mM NaCl and 6 mM $MgCl_2$) was applied through the flow cell before applying a 0.2 mg/ml streptavidin in buffer A for 1 min. Excess streptavidin was removed with 100 μl of buffer A before incubating a 50 pM biotin–DNA substrate. Finally, the flow cell was washed with 100 μl of buffer A to remove unbound DNA. Fluorescence measurements were performed in an imaging buffer consisting of 50 mM Tris-HCl, pH 8.0, 6 mM $MgCl_2$, 20 nM of RT-Cy3, 2 mM trolox, 0.2% triton-X100 and an oxygen scavenging system (0.3 mg/ml glucose oxidase and 40 μg/ml catalase with 5% (w/v) glucose as a substrate). Additionally, PEG 8K was used as a crowding agent and NaCl was used to vary the salt concentration. Where needed, the concentrations of NaCl and PEG 8K are mentioned.

RESULTS

Rapid flipping of RT on a 19-bp double primer dsDNA

Previously, smFRET was used to show that RT spontaneously flips 180° on various nucleic acids (8–10). To study the mechanism of flipping, we immobilized a 19-bp double primed dsDNA (dpdsDNA) (Figure 1B) in which both strands can serve as primer or template (see Supplementary Material for DNA sequences). The symmetric structure of dpdsDNA substrate allows RT to bind in two different orientations (Figure 1B), and the two binding orientations should occur with roughly equal probability. We first examined the binding of RT on dpdsDNA using smFRET under low salt concentration (50 mM NaCl) and low crowding (0% PEG 8k) conditions. Time trajectories showed that on this substrate, RT bound in distinct states with corresponding FRET values of about 0.3 and 1 (Figure 1C).

A histogram of more than 1500 binding events shows that RT spends roughly the same amount of time in each FRET state (Figure 1D). Moreover, RT was observed to flip spontaneously between the two binding modes (indicated with arrows in Figure 1C). Measuring the binding dynamics allowed us to directly measure the frequency of binding and the binding dwell times, which are direct measures of k_{on} and k_{off}, respectively (Supplementary materials). Using this assay we next sought to explore how salt and crowding conditions influence the stability of RT binding to DNA.

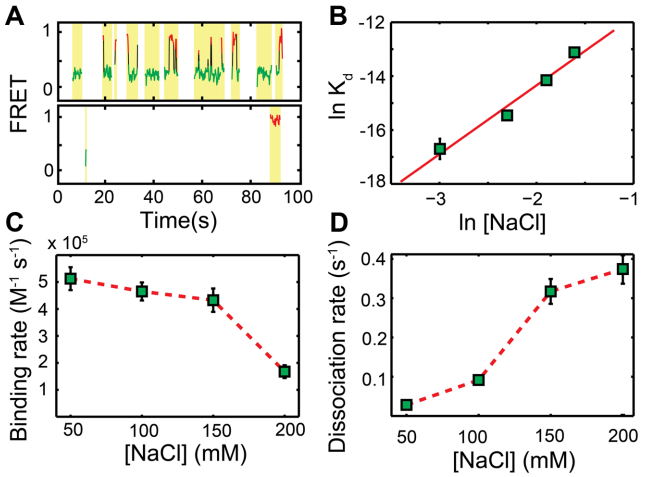

Figure 2. Binding kinetics of RT on DNA as a function of salt concentration. (**A**) Example FRET traces of RT binding dynamics on dpds-DNA. Top: binding dynamics at 50 mM NaCl, bottom: at 200 mM NaCl. Green and red represent a low FRET and high FRET bound states. Black line represents a flipping transition between the two bound states. Yellow shaded region identifies the bound state. (**B**) NaCl linkages ($\partial \ln K_d$ versus $\partial \ln[NaCl] \partial \ln K_d$ versus $\partial \ln[NaCl]$) for the binding of RT to 19-bp dpds-DNA. The slope of the linear fit (red line) to the data (squares) is 2.55, the thermodynamic net average number of ions released upon RT–DNA complex formation. (**C**) Salt concentration dependent binding rate calculated from the frequency of RT binding to DNA over the observation time. (**D**) Salt concentration dependent dissociation rate derived from the dwell times of RT binding. Dashed red line is a reference line connecting the data points. Number of binding events analyzed for 50, 100, 150 and 200 mM salt concentrations are 1534, 2700, 4431 and 659, respectively.

RT binds weakly on DNA under increased ionic concentration

The interactions of a protein–nucleic acid complex are in general strongly influenced by the salt concentration of the buffer. Typically, proteins interact weakly with DNA under high salt concentrations (16,22). The ability of RT to bind to DNA under increased salt concentration was first probed using a bulk primer-extension assay (Supplementary Material). We tested the ability of RT to extend a Cy5-labeled 19-bp DNA primer on a 52-bp template under various salt (NaCl) concentrations (50 and 300 mM). This primer-extension assay revealed that the initial bound fraction of DNA molecules decreased with an increased salt concentration (Supplementary Figure S2), which suggests that screening of ionic charges weakens the binding of RT to DNA templates.

To complement the ensemble results that RT binds less tightly on DNA under increased salt concentration, and to acquire the individual kinetic parameters of flipping and dissociation, we returned to the smFRET assay, which allows precise determination of the dissociation constant (K_d), k_{on}, k_{off} and k_f. These quantities were corrected for the effects of photo-bleaching (Supplementary Material).

Using smFRET we next measured binding of RT on DNA under increased salt concentration. RT exhibited increased dwell times with a higher frequency of binding events at 50 mM NaCl compared to a salt concentration relevant to *in vivo* conditions (150–200 mM NaCl) (Figure 2A and Supplementary Figure S3). Analysis of a large set of single molecule traces (>500 traces in each test condition) demonstrates that K_d increases with an increase in salt concentration (Figure 2B). We also determined the thermodynamic linkage number (L_n) of the interaction which is a measure of binding affinity, given by:

$$L_n = \partial \left(\frac{\ln (K_d)}{\ln [NaCl]} \right) \quad (1)$$

L_n roughly corresponds to the number of counter ions released during formation of a protein–DNA complex (16,34,35). A linear fit to the linkage plot yielded an L_n of 2.5 (Figure 2B). This net release of ions is similar to what was observed for other DNA polymerases (16). The single-molecule results therefore confirm that RT binds weakly under increased salt concentrations.

Next, we estimated the binding and dissociation rates from single-molecule binding events (Supplementary materials) to identify the origin of the change in K_d. k_{off} increased and k_{on} decreased with increased salt concentration (Figure 2C and D), indicating that the transition state corresponding to binding and dissociation shifted relative to both the bound state and the dissociated state. We note that at a salt concentration relevant to *in vivo* conditions, RT binds DNA infrequently and dissociates rapidly once bound. Given that RT copies ~9.8 kilobases of double stranded DNA *in vivo*, we therefore expect cellular conditions stabilize bound RT through some other mechanism.

Impact of macromolecular crowding on binding of RT to DNA

We next investigated if macromolecular crowding is a key factor in determining RT binding stability at a salt concentration that is representative of *in vivo*. We chose a widely-used crowding agent (21,36), PEG 8K, whose radius of gyration is comparable to the length of RT (37). We measured binding dynamics on DNA at 150 mM NaCl under various PEG 8K concentrations using both the bulk primer-extension assay (Supplementary Material) and sm-FRET. With increasing PEG 8K concentration, the fraction of bound DNA increased as measured by the primer-extension assay. The results suggest that increasing the volume fraction occupied by the PEG 8K molecules leads to an increase in the binding stability of RT on DNA (Supplementary Figure S2). Similar increases in stability were observed when other crowding molecules were used (Supplementary Figure S2D).

In order to confirm this relationship, smFRET measurements of RT–DNA interactions in the presence of PEG 8K were performed at 150 mM NaCl. Addition of 10% (w/v) PEG 8K led to an increase in both the binding frequency and dwell times compared to the dilute conditions (Figure 3A, Supplementary Figure S3). We found that increasing the volume fraction of PEG 8K to 10% caused an order of magnitude decrease (i.e. tightening) in K_d (Figure 3B). In addition, a small but measurable increase in k_{on} of RT (Figure 3C) and decrease in k_{off} was observed as crowding increased (Figure 3D).

To determine the binding affinity of RT at *in vivo* crowding conditions, we fit the decrease in the K_d of RT–DNA using scaled-particle theory (21,38,39). This theory predicts that the more compact RT–DNA complex is entropically

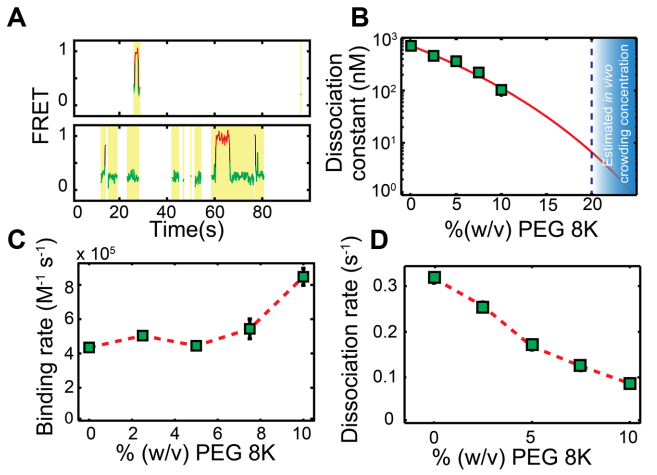

Figure 3. Effects of increased macromolecular crowding on the binding kinetics of RT on dpdsDNA. (**A**) representative FRET traces of RT binding dynamics on dpdsDNA. Top: data obtained at 150 mM NaCl, bottom: data obtained at 150 mM NaCl and 10% (w/v) PEG 8K. Flipping (black line) of RT between low FRET (green) and high FRET (red) is pronounced under increased crowding. Yellow shaded region identifies the bound state. (**B**) Dissociation constant (K_d) of RT binding on DNA under macromolecular crowding. Red curve is a fit to the data (squares) based on scaled particle theory. Blue region is where the concentration of cellular crowding falls in which RT is estimated to have sub-nanomolar binding affinity. (**C** and **D**) Rate of binding and dissociation of RT binding on DNA as a function of PEG 8K at 150 mM NaCl, respectively. Dashed red line is a reference line connecting the data points. Number of binding events analyzed for 0, 2.5, 5, 7.5 and 10% (w/.v) PEG 8K concentrations are 4431, 3925, 4120, 911 and 1049, respectively.

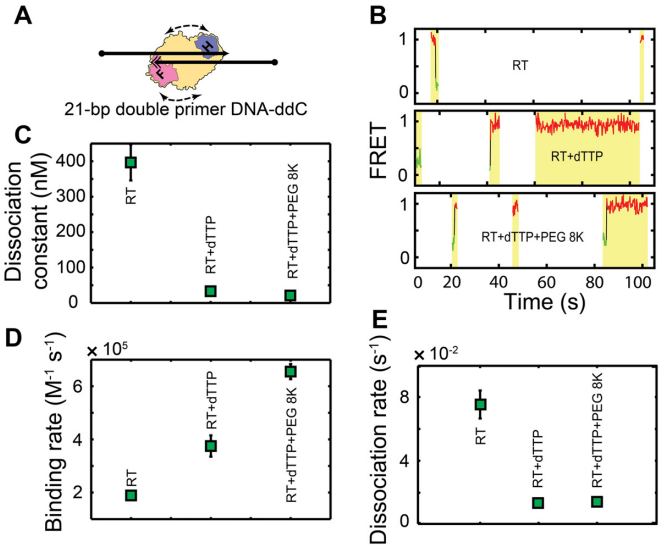

Figure 4. Binding dynamics of RT on 21-bp dpdsDNA with an incoming dNTP. (**A**) A 21-bp double primer DNA construct with a chain-terminating (ddC) priming end (double arrow) to study the effects of an incoming nucleotide on RT binding kinetics. (**B**) Representative FRET traces of RT binding dynamics on 21-bp double primer with a chain terminating dNTP. Top: RT binding under 150 mM NaCl, middle: 150 mM NaCl and 250 μM dTTP and bottom: 150 mM NaCl, 250 μM dTTP and 7.5% PEG 8K, respectively. Yellow shaded region identifies the bound state. (**C**) Dissociation constant of RT binding on 21-bp DNA-ddC. (**D** and **E**) Rate of binding and rate of dissociation of RT on 21-bp DNA-ddC. Number of binding events analyzed for RT, RT+dTTP and RT+dTTP+PEG 8K are 393, 284 and 471, respectively.

favored over the dissociated RT and DNA as the number of crowding molecules increases. By modeling the DNA, RT and the RT–DNA complex with simple geometric forms approximating their size and shape (Supplementary Material), we find we can fit the relative decrease in the dissociation constant without any additional free parameters (Figure 3B). Extrapolation of this curve to physiological crowding conditions suggests RT binds with a sub-nanomolar dissociation constant *in vivo*. We also measured the effects of crowding at 200 mM NaCl with similar results (Supplementary Figure S4). We therefore find that the effects of macromolecular crowding on the dissociation constant of RT can be interpreted straightforwardly from the entropic effects described in scaled particle theory.

Because increased macromolecular crowding also increases the viscosity of solution, we tested the effect of viscosity on the binding of RT to DNA independently. We used high concentrations of D-(+)-dextrose in order to create a similar effective viscosity. We did not observe a significant difference in K_d under increased D-(+)-dextrose concentration (Supplementary Figure S5A). However, a decrease in k_{on} and k_{off} was observed (Supplementary Figure S6B and S6C). These results indicate that the increased viscosity due to increased crowing could only have slowed the kinetics of binding and dissociation slightly, but did not affect the stability of the bound complex.

RT binds stably on DNA with an incoming nucleotide

Both salt concentration and crowding can alter the attraction of RT and DNA even at longer ranges (∼1 nm separation). In order to increase in the stability of RT–DNA complexes without stabilizing the transition states, we examined the binding in the presence of cognate nucleotides (dNTP). Previously, an RT/DNA/dNTP ternary complex was shown to have higher stability than RT/DNA alone (8). We therefore prepared a new double primer DNA of 21-bp with a chain terminating nucleotide (dideoxynucleotide) at one of the 3′-priming ends (Figure 4A and see Supplementary Material for DNA sequences). In the absence of this nucleotide, the binding kinetics of RT on this substrate was comparable to the standard dpdsDNA (compare Figure 2A, bottom and Figure 4B, top). The addition of 250 μM dTTP (the next cognate nucleotide for the high FRET orientation) lead to RT binding predominantly in a high FRET state (Figure 4B, middle). Since the addition of nucleotides lead to stabilization of high FRET state only, we only compared the high FRET data on this substrate. As expected, the presence of cognate nucleotides greatly decreased the effective K_d (Figure 4C). This was caused primarily by a decrease in k_{off} rather than an increase in k_{on} (Figure 4D and E). We also explored the combined effects of 250 μM dTTP and 7.5% (w/v) PEG 8K, and found that binding was further stabilized. Under these conditions, k_{on} increased significantly and k_{off} decreased significantly compared to RT alone (Figure 4). We conclude that short-range interactions primarily change k_{off} rather than k_{on}.

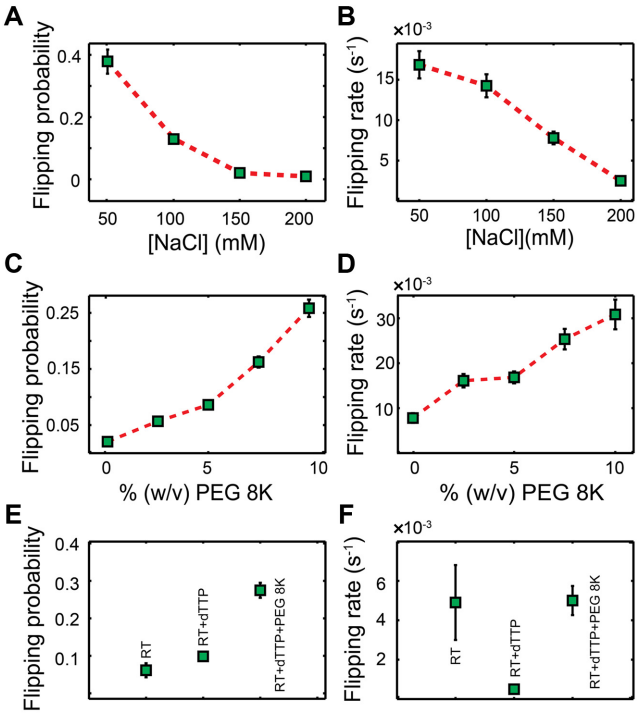

Figure 5. Effects of increased salt concentration and macromolecular crowding on the flipping transition of RT. (**A**) NaCl dependence of probability of flipping of RT on 19-bp double primer. (**B**) NaCl dependence of rate of flipping. (**C**) PEG 8K dependence of probability of flipping of RT at 150 mM NaCl. (**D**) PEG 8K dependence of rate of flipping of RT at 150 mM NaCl. (**E**) Probability of flipping of RT on 21-bp double primer DNA-ddC (Figure 4A). (**F**) Rate of flipping of RT on 21-bp double primer.

Increased ionic concentration makes flipping less likely

Having established the effect of salt concentration and crowding on the bound states, we next wanted to explore how the flipping transition state responded to these conditions. These measurements can determine the strength of ionic interactions and the degree of compaction in the transition states and any short-lived intermediate states involved in flipping. We again analyzed binding events as a function of salt concentration (Figure 2A), but we now extracted the effective k_f, i.e. the number of flipping events per second bound, and P_{flip}, i.e. likelihood of flipping versus dissociation from a high or low FRET event (Supplementary materials). The P_{flip} is determined solely by the ratio of k_f and k_{off}. While increasing salt concentration increased k_{off}, the number of flipping events dropped dramatically (Figure 2A). P_{flip} dropped monotonically with increased salt concentration, with a total decrease of >98% from 50 mM to 200 mM (Figure 5A). This sharp decrease in P_{flip} can be partly attributed to the increase in k_{off}. However, k_f also dramatically decreased as the salt concentration was increased (Figure 5B). As a whole, k_f at 200 mM NaCl decreased by >95% compared to 50 mM NaCl. These results indicate that k_f and k_{off} move in opposite directions in response to salt concentration.

Flipping is more likely in the presence of crowding agents

We next extracted k_f and P_{flip} from binding events measured in the presence of crowding agents (Figure 3A). A monotonic increase in P_{flip} was observed as the PEG 8K concentration increased from 0% to 10% (Figure 5C). Addition of 10% (w/v) PEG 8K resulted in a 10-fold increase in P_{flip}. We also found that while k_{off} decreased in the presence of crowding agents, k_f consistently increased (Figure 5D). Taken together, we once again see that k_f moves in the opposite direction from k_{off} with crowding. It also indicates that flipping occurs frequently at *in vivo* salt and crowding conditions.

Flipping is equally likely but less frequent in the presence of cognate dNTP

Finally, we wished to determine how flipping was influenced when no long range attractive potential exists but the stability of the bound state is altered. We extracted k_f and P_{flip} from high FRET binding in the presence of 250 μM cognate dNTP (Figure 4B). While P_{flip} was minimally affected, k_f decreased dramatically (Figure 5D and F). This indicates that k_f and the k_{off} scaled together, keeping P_{flip} roughly constant. Addition of dTTP and 7.5% PEG 8K further stabilized the binding, but increased P_{flip} and k_f. We conclude from this that short-range stabilization of the RT bound state affects k_f and k_{off} identically. Taken together, these results suggest that long-range forces are likely the cause of the differential effects in k_f and k_{off} observed under different salt and crowding conditions.

DISCUSSION

Flipping is an important transition, allowing proteins to rapidly find specific targets on nucleic acid substrates. We considered two potential mechanistic models of flipping, 'tumbling' and 'hopping'. A key difference between our models is that k_f competes with k_{off} directly from the bound state in the tumbling model, while hopping requires dissociation into a pseudo-bound state that allows the RT to rebind or fully dissociate (Figure 1A).

We describe both the tumbling and hopping models using Markov chains (Figure 1A). Each model has exactly three free parameters that can describe the flipping behavior. These free parameters can be related to the experimentally measured parameters (the rate constants of binding, dissociation and flipping) (Table 1). In the case of tumbling, each rate constant from the model corresponds directly to a measured rate constant. In the hopping model, we assumed the pseudo-bound state was too short lived to contribute directly to bound lifetimes. Therefore, the behavior was entirely described by the two rate constants of entering into the pseudo-bound state and the ratio of the rates exiting the pseudo-bound state, i.e. the branching ratio r. The relationships between these three free parameters and the measured rate constants were derived (Supplementary Material and Table S1). Based on the derived rate constants, we calculated the associated free energy diagrams for each model at both 50 mM and 200 mM NaCl with 0% PEG 8K (Figure 6, orange and black lines). A similar set of diagrams was

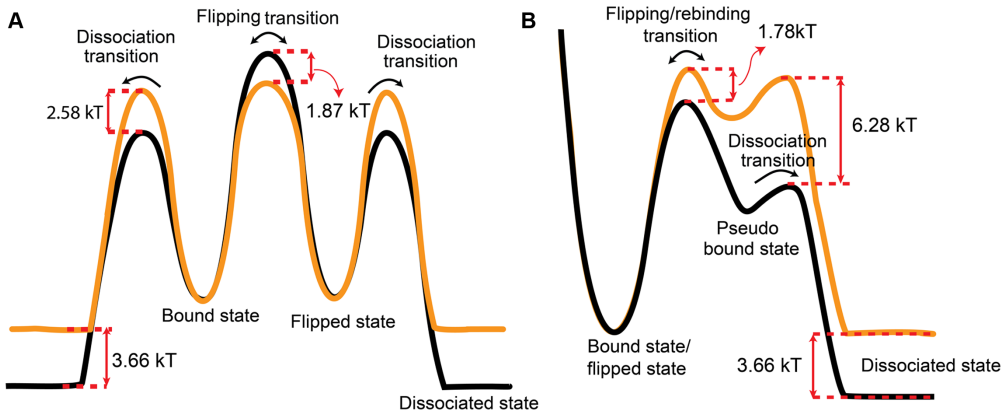

Figure 6. Free energy diagrams of RT flipping kinetics on DNA. The free energy diagrams were drawn for tumbling model and hopping model based on the kinetic and thermodynamic data obtained under different NaCl concentrations. (**A**) Free energy diagram corresponding to the tumbling model of RT binding and flipping kinetics under high salt concentration (black). Decreased salt concentration leads to increase in the free energy barrier height for dissociation transition and decrease in the barrier height for flipping transition relative to the bound or flipped bound state (orange). (**B**) Free energy diagram explaining flipping kinetics based on hopping model with an extra pseudo-bound state. In this free energy diagram both the bound state and flipped state are identical. Color convention is the same as in the free energy diagram for tumbling model.

generated for 150 mM NaCl at 0% and 10% PEG 8K (Supplementary Figure S6, black and orange lines). In the hopping model, we have used the same energy well to represent both the bound state and the flipped state, since these states are roughly symmetric on our DNA substrate. We aligned these free energy diagrams so that the energy of the bound state was the same under each buffer condition.

If crowding and salt concentration only affected the stability of the bound states, then in both models we would expect k_{off} to scale with k_f and P_{flip} to remain constant, as was observed when cognate nucleotide was added to solution. However, if crowding and salt concentration also influence the stability of the transition states, then the P_{flip} can change as well. Our data reveal that the P_{flip} did not remain constant in these two cases. Instead, decreased salt concentration or increased crowding increased the P_{flip} (Figure 5A and C). This shows that the transition states are affected by the changes in the buffer conditions, and the manner in which P_{flip} changes supports the hopping model.

First, we discuss why the tumbling model has difficulties explaining the data. In the tumbling model, k_f is expected to increase with ionic concentration because the tumbling transition state should break some of the ionic contacts that are present between RT and DNA in the bound state (40,41). Instead, we observed that k_f decreased as the salt concentration increased. k_f was also expected to decrease with increased crowding because the tumbling transition state should become less compact compared to the bound state. Instead, we observed that k_f increased as the volume fraction of PEG 8K increased. If we use a tumbling model to fit our experimental data, we therefore have to conclude that the flipping transition is more destabilized by increased salt concentration relative to the bound state (Figure 6A). Conversely, the flipping transition would have to be stabilized by increased crowding (Supplementary Figure S7A). This would suggest an unphysical transition state that is both more compact and has more electrostatic contacts between the RT and DNA than the bound state.

Next, we discuss why the hopping model is consistent with our experimental observations. The hopping model assumes that the macromolecular complexes undergo many short-lived diffusive excursions and re-bindings before a complete dissociation can occur. These short-lived excursions are kinetically equivalent to a pathway where RT must move from the bound state to a pseudo-bound state before dissociating (26) (Figure 1A). When RT enters the short-lived pseudo-bound state, it has a chance to dissociate or to rebind in either the original orientation or a flipped orientation. For simplicity and because our DNA template is nearly symmetric, we assume there is an equal chance of rebinding in flipped state or in the original orientation. Decreasing salt concentration or increasing crowding should create more long-range attractive forces between RT and DNA (42,43). We expect that these long-range attractive forces should increase the chance of rebinding relative to the chance of dissociation from the pseudo-bound state. To provide support for this assumption, we numerically simulated the Brownian motion of two spherical particles in close proximity. In the presence of an attractive force extending for ~2 nm from each particle, both the number and frequency of diffusive excursions taking the particles more than 7 nm apart (the diameter of RT) before they came into contact again increased (Supplementary Figure S7).

Therefore, we expect P_{flip} and k_f to increase as the salt concentration is decreased or crowding is increased, as we observe in the data. Fitting our experimental data to the hopping model, we in fact observe that at lower salt concentrations the rebinding/flipping transition is destabilized by a smaller amount than the dissociation transition (Figure 6B). A similar result is derived from the crowding data (Supplementary Figure S6B). Therefore, we conclude that flipping proceeds by hopping rather than tumbling.

In addition to this primary conclusion, our research demonstrates that macromolecular crowding plays a major role in determining how strongly RT binds nucleic acids. *In vitro* experiments on RT, both in bulk and at single-molecule level, are frequently performed in dilute solutions with low

Table 1. Equations describing probability of flipping and rate of flipping for tumbling and hopping model

	Tumbling model	Hopping model
Rate constant of dissociation (k_{off})	$k_{B\rightarrow D}$	$k_{B\rightarrow P}(\frac{1+r}{2+r})$
Rate constant of flipping (k_f)	$k_{B\rightarrow F}$	$\frac{k_{B\rightarrow P}}{2+r}$
Rate constant of binding (k_{on})	$k_{D\rightarrow B}$	$\frac{k_{D\rightarrow P}}{2+r}$

r is the branching ratio defined by: $r = \frac{k_{P\rightarrow D}}{k_{P\rightarrow B}}$.

salt concentration (32,44). This contrasts with the crowded and salty milieu inside cells and viruses, with around 200–400 mg/ml of different macromolecules and effective salt concentrations of ∼150 mM (45–49). In line with previous findings on crowding-induced effects on the stability of DNA binding proteins (19,22), we find that increased crowding at salt concentrations relevant to those found *in vivo* can result in comparable binding affinities to those achieved at low salt concentrations under dilute conditions (Figures 2 and 3). In fact, fitting K_d to scaled-particle theory suggests that RT binds DNA with a sub-nanomolar K_d at physiological crowding conditions. We therefore emphasize that crowding is an important variable to control when trying to predict *in vivo* rates from *in vitro* data, particularly when predicting the effects of antiretroviral drugs on the efficiency of reverse transcription.

Our results have implication for other macromolecular complexes as well. The fact that flipping of RT can be modeled through hopping and rebinding is consistent with the recent observation that macromolecular DNA complexes rebind after entering a pseudo-bound state, allowing the bound lifetime to be shortened by competitive inhibition (26). Indeed, any physical model of the dissociation of two diffusing macromolecules would imply that some rebinding should occur with a finite probability, since the free molecules undergo a random walk. Our observations provide empirical evidence that these short excursions can allow flipping to occur before the molecules rebind.

The highly crowded environment inside the cell provides long-range attractive interactions between many binding macromolecules similar to those provided by our *in vitro* crowding agents, increasing the probability of rebinding and flipping. This increase means that for any encounter between two macromolecules, a wider range of configurations can be explored through rebinding before complete dissociation occurs. This exploration can make the assembly of macromolecular complexes kinetically more efficient (50,51). Rebinding and flipping also aids enzymes that perform more than one reaction per encounter, such as DNA polymerases that contain an exonuclease site (52), type II restriction enzymes (4–6) or ERK phosphorylation by MEK (53,54). We have demonstrated that smFRET combined with kinetic analysis provides a useful tool for exploring the role rebinding and flipping play in all of these systems.

SUPPLEMENTARY DATA

Supplementary Data are available at NAR Online.

ACKNOWLEDGEMENTS

The authors thank Anna Haagsma for her technical support. The authors thank Chirlmin Joo, Luuk Leoff, Misha Klein and Maarten van Oene for their critical reading this manuscript.

FUNDING

Marie Curie Career Integration Grant [304284]; Nanofront initiative of the Netherlands Organization for Scientific Research [NWO, NF13BNS01]; Department of Bionanoscience of the Delft University of Technology; Intramural Research Program of the National Cancer Institute, National Institutes of Health, Department of Health and Human Services [to S.F.J.L.G]. Funding for open access charge: Department of Bionanoscience of the Delft University of Technology.
Conflict of interest statement. None declared.

REFERENCES

1. Berg,O.G., Winter,R.B. and Von Hippel,P.H. (1981) Diffusion-driven mechanisms of protein translocation on nucleic acids. 1. Models and theory. *Biochemistry*, **20**, 6929–6948.
2. Berg,O.G. and von Hippel,P.H. (1985) Diffusion-Controlled Macromolecular Interactions. *Annu. Rev. Biophys. Biophys. Chem.*, **14**, 131–158.
3. Halford,S.E. and Marko,J.F. (2004) How do site-specific DNA-binding proteins find their targets? *Nucleic Acids Res.*, **32**, 3040–3052.
4. Sasnauskas,G., Kostiuk,G., Tamulaitis,G. and Siksnys,V. (2011) Target site cleavage by the monomeric restriction enzyme BcnI requires translocation to a random DNA sequence and a switch in enzyme orientation. *Nucleic Acids Res.*, **39**, 8844–8856.
5. Sasnauskas,G., Zakrys,L., Zaremba,M., Cosstick,R., Gaynor,J.W., Halford,S.E. and Siksnys,V. (2010) A novel mechanism for the scission of double-stranded DNA: BfiI cuts both 3′–5′ and 5′–3′ strands by rotating a single active site. *Nucleic Acids Res.*, **38**, 2399–2410.
6. Pingoud,A., Wilson,G.G. and Wende,W. (2014) Type II restriction endonucleases—a historical perspective and more. *Nucleic Acids Res.*, **42**, 7489–7527.
7. Ryu,K.-S., Tugarinov,V. and Clore,G.M. (2014) Probing the rate-limiting step for intramolecular transfer of a transcription factor between specific sites on the same DNA molecule by 15Nz-exchange NMR spectroscopy. *J. Am. Chem. Soc.*, **136**, 14369–14372.
8. Abbondanzieri,E.A., Bokinsky,G., Rausch,J.W., Zhang,J.X., Le Grice,S.F.J. and Zhuang,X. (2008) Dynamic binding orientations direct activity of HIV reverse transcriptase. *Nature*, **453**, 184–189.
9. Liu,S., Abbondanzieri,E.A., Rausch,J.W., Le Grice,S.F.J. and Zhuang,X. (2008) Slide into Action: Dynamic shuttling of HIV reverse transcriptase on nucleic acid substrates. *Science*, **322**, 1092–1097.
10. Liu,S., Harada,B.T., Miller,J.T., Le Grice,S.F.J. and Zhuang,X. (2010) Initiation complex dynamics direct the transitions between distinct phases of early HIV reverse transcription. *Nat. Struct. Mol. Biol.*, **17**, 1453–1460.

11. Sharma,K.K., Przybilla,F., Restle,T., Godet,J. and Mély,Y. (2016) FRET-based assay to screen inhibitors of HIV-1 reverse transcriptase and nucleocapsid protein. *Nucleic Acids Res.*, **44**, e74.
12. Sharma,K.K., Przybilla,F., Restle,T., Boudier,C., Godet,J. and Mély,Y. (2015) Reverse transcriptase in action: FRET-based assay for monitoring flipping and polymerase activity in real time. *Anal. Chem.*, **87**, 7690–7697.
13. Blainey,P.C., Luo,G., Kou,S.C., Mangel,W.F., Verdine,G.L., Bagchi,B. and Xie,X.S. (2009) Nonspecifically bound proteins spin while diffusing along DNA. *Nat. Struct. Mol. Biol.*, **16**, 1224–1229.
14. Zheng,Q., Juette,M.F., Jockusch,S., Wasserman,M.R., Zhou,Z., Altman,R.B. and Blanchard,S.C. (2014) Ultra-stable organic fluorophores for single-molecule research. *Chem. Soc. Rev.*, **43**, 1044–1056.
15. Kong,X., Nir,E., Hamadani,K. and Weiss,S. (2007) Photobleaching pathways in single-molecule FRET experiments. *J. Am. Chem. Soc.*, **129**, 4643–4654.
16. Datta,K. and LiCata,V.J. (2003) Salt dependence of DNA binding by Thermus aquaticus and Escherichia coli DNA polymerases. *J. Biol. Chem.*, **278**, 5694–5701.
17. Akabayov,B., Akabayov,S.R., Lee,S.-J., Tabor,S., Kulczyk,A.W. and Richardson,C.C. (2010) Conformational dynamics of bacteriophage T7 DNA polymerase and its processivity factor, Escherichia coli thioredoxin. *Proc. Natl. Acad. Sci. U.S.A.*, **107**, 15033–15038.
18. Minton,A.P. (1981) Excluded volume as a determinant of macromolecular structure and reactivity. *Biopolymers*, **20**, 2093–2120.
19. Zimmerman,S.B. and Harrison,B. (1987) Macromolecular crowding increases binding of DNA polymerase to DNA: An adaptive effect. *Proc. Natl. Acad. Sci. U.S.A.*, **84**, 1871–1875.
20. Ellis,R.J. (2001) Macromolecular crowding: obvious but underappreciated. *Trends Biochem. Sci.*, **26**, 597–604.
21. Zhou,H.-X., Rivas,G. and Minton,A.P. (2008) Macromolecular crowding and confinement: Biochemical, biophysical and potential physiological consequences. *Annu. Rev. Biophys.*, **37**, 375–397.
22. Akabayov,B., Akabayov,S.R., Lee,S.-J., Wagner,G. and Richardson,C.C. (2013) Impact of macromolecular crowding on DNA replication. *Nat. Commun.*, **4**, 1615.
23. Kao-Huang,Y., Revzin,A., Butler,A.P., O'Conner,P., Noble,D. and Von Hippel,P.H. (1977) Nonspecific DNA binding of genome-regulating proteins as a biological control mechanism: Measurement of DNA-bound Escherichia coli lac repressor in vivo. *Proc. Natl. Acad. Sci. U.S.A.*, **74**, 4228–4232.
24. Blainey,P.C., van Oijen,A.M., Banerjee,A., Verdine,G.L. and Xie,X.S. (2006) A base-excision DNA-repair protein finds intrahelical lesion bases by fast sliding in contact with DNA. *Proc. Natl. Acad. Sci. U.S.A.*, **103**, 5752–5757.
25. Farge,G., Laurens,N., Broekmans,O.D., van den Wildenberg,S.M.J.L., Dekker,L.C.M., Gaspari,M., Gustafsson,C.M., Peterman,E.J.G., Falkenberg,M. and Wuite,G.J.L. (2012) Protein sliding and DNA denaturation are essential for DNA organization by human mitochondrial transcription factor A. *Nat. Commun.*, **3**, 1013.
26. Paramanathan,T., Reeves,D., Friedman,L.J., Kondev,J. and Gelles,J. (2014) A general mechanism for competitor-induced dissociation of molecular complexes. *Nat. Commun.*, **5**, 5207.
27. Bonnet,I., Biebricher,A., Porté,P.-L., Loverdo,C., Bénichou,O., Voituriez,R., Escudé,C., Wende,W., Pingoud,A. and Desbiolles,P. (2008) Sliding and jumping of single EcoRV restriction enzymes on non-cognate DNA. *Nucleic Acids Res.*, **36**, 4118–4127.
28. Gowers,D.M., Wilson,G.G. and Halford,S.E. (2005) Measurement of the contributions of 1D and 3D pathways to the translocation of a protein along DNA. *Proc. Natl. Acad. Sci. U.S.A.*, **102**, 15883–15888.
29. Le Grice,S.F.J., Cameron,C.E. and Benkovic,S.J. (1995) Purification and characterization of human immunodeficiency virus type 1 reverse transcriptase. *Methods Enzymol.*, **262**, 130–144.
30. Schatz,O., Cromme,F.V., Grüninger-Leitch,F. and Le Grice,S.F.J. (1989) Point mutations in conserved amino acid residues within the C-terminal domain of HIV-1 reverse transcriptase specifically repress RNase H function. *FEBS Lett.*, **257**, 311–314.
31. Rausch,J.W., Sathyanarayana,B.K., Bona,M.K. and Le Grice,S.F.J. (2000) Probing contacts between the ribonuclease H domain of HIV-1 reverse transcriptase and nucleic acid by site-specific photocross-linking. *J. Biol. Chem.*, **275**, 16015–16022.
32. Marko,R.A., Liu,H.-W., Ablenas,C.J., Ehteshami,M., Götte,M. and Cosa,G. (2013) Binding kinetics and affinities of heterodimeric versus homodimeric HIV-1 reverse transcriptase on DNA–DNA substrates at the single-molecule level. *J. Phys. Chem. B*, **117**, 4560–4567.
33. Chandradoss,S.D., Haagsma,A.C., Lee,Y.K., Hwang,J.H., Nam,J.M. and Joo,C. (2014) Surface passivation for single-molecule protein studies. *J. Vis. Exp.*, **86**, e50549.
34. Wyman,J. Jr (1964) Linked functions and reciprocal effects in hemoglobin: a second look. *Adv. in Protein Chem.*, **19**, 223–286.
35. Record,M.T. Jr, Ha,J.-H. and Fisher,M.A. (1991) Analysis of equilibrium and kinetic measurements to determine thermodynamic origins of stability and specificity and mechanism of formation of site-specific complexes between proteins and helical DNA. *Methods Enzymol.*, **208**, 291–343.
36. Dupuis,N.F., Holmstrom,E.D. and Nesbitt,D.J. (2014) Molecular-crowding effects on single-molecule RNA folding/unfolding thermodynamics and kinetics. *Proc. Natl. Acad. Sci. U.S.A.*, **111**, 8464–8469.
37. Thiyagarajan,P., Chaiko,D.J. and Hjelm,R.P. (1995) A Neutron Scattering Study of Poly(ethylene glycol) in Electrolyte Solutions. *Macromolecules*, **28**, 7730–7736.
38. Reiss,H., Frisch,H.L. and Lebowitz,J.L. (1959) Statistical Mechanics of Rigid Spheres. *J. Chem. Phys.*, **31**, 369–380.
39. Lebowitz,J.L., Helfand,E. and Praestgaard,E. (1965) Scaled particle theory of fluid mixtures. *J. Chem. Phys.*, **43**, 774–779.
40. Ding,J., Das,K., Hsiou,Y., Sarafianos,S.G., Clark,A.D. Jr, Jacobo-Molina,A., Tantillo,C., Hughes,S.H. and Arnold,E. (1998) Structure and functional implications of the polymerase active site region in a complex of HIV-1 RT with a double-stranded DNA template-primer and an antibody fab fragment at 2.8 Å resolution1. *J. Mol. Biol.*, **284**, 1095–1111.
41. Sarafianos,S.G., Das,K., Tantillo,C., Clark,A.D., Ding,J., Whitcomb,J.M., Boyer,P.L., Hughes,S.H. and Arnold,E. (2001) Crystal structure of HIV-1 reverse transcriptase in complex with a polypurine tract RNA:DNA. *EMBO J.*, **20**, 1449–1461.
42. Vologodskii,A. and Cozzarelli,N. (1995) Modeling of long-range electrostatic interactions in DNA. *Biopolymers*, **35**, 289–296.
43. Yodh,A.G., Lin,K., Crocker,J.C., Dinsmore,A.D., Verma,R. and Kaplan,P.D. (2001) Entropically driven self–assembly and interaction in suspension. *Philos. Trans. R. Soc. Lond. A* **359**, 921–937.
44. Schauer,G.D., Huber,K.D., Leuba,S.H. and Sluis-Cremer,N. (2014) Mechanism of allosteric inhibition of HIV-1 reverse transcriptase revealed by single-molecule and ensemble fluorescence. *Nucleic Acids Res.* **42**, 11687–11696.
45. Fulton,A.B. (1982) How crowded is the cytoplasm? *Cell*, **30**, 345–347.
46. Spitzer,J. (2011) From water and ions to crowded biomacromolecules: In vivo structuring of a prokaryotic cell. *Microbiol. Mol. Biol. Rev.*, **75**, 491–506.
47. del Álamo,M., Rivas,G. and Mateu,M.G. (2005) Effect of macromolecular crowding agents on human immunodeficiency virus Type 1 Capsid protein assembly in vitro. *J. Virol.*, **79**, 14271–14281.
48. Briggs,J.A.G., Simon,M.N., Gross,I., Krausslich,H.-G., Fuller,S.D., Vogt,V.M. and Johnson,M.C. (2004) The stoichiometry of Gag protein in HIV-1. *Nat. Struct. Mol. Biol.*, **11**, 672–675.
49. Benjamin,J., Ganser-Pornillos,B.K., Tivol,W.F., Sundquist,W.I. and Jensen,G.J. (2005) Three-dimensional structure of HIV-1 Virus-like particles by electron cryotomography. *J. Mol. Biol.*, **346**, 577–588.
50. Fange,D., Berg,O.G., Sjöberg,P. and Elf,J. (2010) Stochastic reaction-diffusion kinetics in the microscopic limit. *Proc. Natl. Acad. Sci. U.S.A.*, **107**, 19820–19825.
51. Lomholt,M.A., Zaid,I.M. and Metzler,R. (2007) Subdiffusion and weak ergodicity breaking in the presence of a reactive boundary. *Phys. Rev. Lett.*, **98**, 200603–200606.
52. Wuite,G.J.L., Smith,S.B., Young,M., Keller,D. and Bustamante,C. (2000) Single-molecule studies of the effect of template tension on T7 DNA polymerase activity. *Nature*, **404**, 103–106.
53. Takahashi,K., Tănase-Nicola,S. and ten Wolde,P.R. (2010) Spatio-temporal correlations can drastically change the response of a MAPK pathway. *Proc. Natl. Acad. Sci. U.S.A.*, **107**, 2473–2478.
54. Aoki,K., Takahashi,K., Kaizu,K. and Matsuda,M. (2013) A quantitative model of ERK MAP kinase phosphorylation in crowded media. *Sci. Rep.*, **3**, 1541.